Journal of King Saud University – Science 34 (2022) 101724

Contents lists available at ScienceDirect

Journal of King Saud University – Science

journal homepage: www.sciencedirect.com

# Synergistic effect of silver doped ZnO nanomaterials enhances the anticancer potential against A459 lung cancer cells

Asmat Ullah [a], Malik Saadullah [b,*], Farah Alvi [c], Lubna Sherin [d], Akbar Ali [c,*], Naveed Akhtar Shad [e], Yasir Javed [a,*], M. Munir Sajid [f], Ghulam Yasin [g], Wasim Abbas [e]

[a] Department of Physics, University of Agriculture, Faisalabad, Pakistan
[b] Department of Pharmaceutical Chemistry, GC University Faisalabad, Pakistan
[c] Department of Physics, COMSATS Institute University, Lahore Campus, Islamabad, Pakistan
[d] Department of Chemical Engineering, COMSATS Institute University, Lahore Campus, Islamabad, Pakistan
[e] National Institute of Biotechnology and Genetic Engineering, Jhang Road, Faisalabad, Pakistan
[f] Henan Key Laboratory of Photovoltaic Materials, School of Physics, Henan Normal University, Xinxiang 453007, China
[g] Department of Physics, Punjab University, Lahore, India

ARTICLE INFO

*Article history:*
Received 25 June 2021
Revised 2 November 2021
Accepted 15 November 2021
Available online 22 November 2021

*Keywords:*
Ag doped ZnO
Nanomaterials
Characterization
Anticancer activity
A459 lungs cancer cells

ABSTRACT

*Objective:* In this study, the zinc oxide (ZnO) and silver (0.3 wt% and 0.6 wt%) doped ZnO nanoparticles (NPs) have been synthesized for studying their anticancer potential against lung cancer cells.
*Methods:* Chemical co-precipitation route is used to synthesized the nanomaterials and characterized by different analytical techniques such as X-rays diffraction (XRD), Raman spectroscopy, Fourier transform infrared spectroscopy (FTIR), scanning electron microscope (SEM), and photoluminescence (PL) spectroscopy. Anticancer activity is evaluated on A459 lung cancer cells.
*Results:* XRD pattern reveals the development of (100), (002) and (101) diffraction peaks related to ZnO hexagonal phase. The change in peak intensity and crystalline size are strongly dependent on the silver contents in the ZnO lattice. The Raman bands appeared at 383, 436 and 578 $cm^{-1}$ wave number are related to ZnO phase confirming the existence of chemical bond between Zn and O. The SEM microstructures reveal the formation of aggregates and flakes like morphologies. Optical absorption of ZnO is blue shifted upon addition of silver atoms.
*Conclusion:* Anticancer activity of synthesized nanomaterials has shown that 0.3 wt% Ag doped ZnO presents higher cell inhibition (72.86%) against A459 lung cancer cells.


## 1. Introduction

In recent years, development of novel drugs for different biological treatments shows inefficiency against infectous diseases but the nanotechnology offered modified drugs which provide better prospects against viral and uncurable cancer types (Herng et al., 2007; Kaur et al., 2017). The ongoing crisis in medical field increases the ineffectiveness of traditional antibiotics in disease organism and nanomaterials based drugs provide better alternative to enhance efficacy (Lam et al., 2018; Kumar et al., 2017). The food and drug-controlled authorities established the ZnO NPs as one of the harmless materials which possess unique physicochemical, optical and biological properties (Chen et al., 2015). Additionally, ZnO has antimicrobial efficiency against fungus, viruses and bacteria (Nagaraju et al., 2017; Ravichandran et al., 2015).

The crystalline semiconductor nanomaterials have remarkable applications in medical field for diagnosis and treatment of different diseases (Chen et al., 2005; Golego et al., 2000). Zinc oxide (ZnO), is a wide energy band gap (3.4 eV) semiconductor material. ZnO NPs, with 60 meV exciton binding energy and lattice parameters, $a$ = 0.325 nm, $c$ = 0.521 nm, have shown potential for both technology and biomedical applications (Keren et al., 2003; Wang et al., 2007). ZnO nanomaterials have applications in trans-

* Corresponding authors.
*E-mail addresses:* maliksaadullah@gcuf.edu.pk (M. Saadullah), drakbar.ali@cui-lahore.edu.pk (A. Ali), myasi60@hotmail.com (Y. Javed).

Peer review under responsibility of King Saud University.

Production and hosting by Elsevier

https://doi.org/10.1016/j.jksus.2021.101724
1018-3647/

parent electronics (Nomura et al., 2003), ultraviolet (UV) blocking creams, light emitting diode (Nakada et al., 2004), piezoelectric devices, chemical sensors and spintronics (Wang and Kong, 2004; Pearton et al., 2004). The ZnO structure can be modified by doping the transition metals such as Mg, Al, Mn, Cu, Ni, Ag to tune the properties of the nanomaterials (Wang et al., 2007). Amid these transition metals, the doping of Ag is more important because this enhances the optical properties of ZnO nanomaterials (Nomura et al., 2003). Silver belongs to transition metal group with high thermal and electrical conductivity. The utilization of silver in medical and therapeutics is very old, however, basic antimicrobial behavior is discovered later. In recent years silver NPs have achieved much attention in medical filed due to its various applications such as antimicrobial, anticancer and antibacterial agent (Beyene et al., 2017). Chauhan et al. (2010) have synthesized Ag doped ZnO NPs by chemical co-precipitation technique showing improved antibacterial properties, antimicrobial and anticancer activates. Noble metal doping in ZnO also exhibited enhanced photocatalytic activity (Caglar and Yakuphanoglu, 2012; Pal et al., 2013) (see Table 1).

The doping process can be performed by thermal treatment or incorporation during chemical reaction (Pal et al., 2013; Pal et al., 2015). At high temperature, silver doped ZnO nanomaterials presents higher stability and similarity with other transparent conducting materials, making these nanomaterials suitable in optoelectronic applications (Mohan et al., 2014). So far, different methods are used to produce doped ZnO nanomaterials such as sol–gel technique (Castro-Lopes et al., 2020), soft chemical route (Naskar et al., 2019), co-precipitation (Sundaram et al., 2019), hydrothermal method (Neto et al., 2019) and solvo-thermal method (Sagadevan et al., 2017) (see Table 2).

In this research work, the role of Ag (0, 0.3%, 0.6%) contents on ZnO nanomaterials synthesized by co-precipitation technique is investigated by following the structural, morphological and optical properties and evaluating nanomaterials as anti-cancer agent.

## 2. Experimental section

### 2.1. Experimental procedure

Zinc acetate dehydrate (Zn $(CH_3CO_2)_2{\cdot}2H_2O$), Silver nitrate ($AgNO_3$), Methanol ($CH_3OH$), sodium hydroxide (NaOH) were purchased from sigma Aldrich through local suppliers and used without any further purification.

**Table 2**
Change in cell dimensions and bond length with silver doping in zinc oxide.

| Phase | Lattice constant | | Bond length |
|---|---|---|---|
| $Ag_x$-$ZnO_{1-x}$ | a (nm) | c (nm) | L (nm) |
| X = 0 | 0.326 | 0.524 | 0.145 |
| X = 0.3 | 0.326 | 0.524 | 0.155 |
| X = 0.6 | 0.327 | 0.526 | 0.159 |

#### 2.1.1. Method

ZnO and Ag doped ZnO NPs in parallel experiment were synthesized by co-precipitation method with Ag concentration (x = 0, 0.3, 0.6 wt%). Initially 3 g (0.24 M) Zinc acetate dehydrate (Zn $(CH_3CO_2)_2{\cdot}2H_2O$) was dissolved in 200 mL of methanol ($CH_3OH$) and stirred vigorously for two hours. In next step, 1 M (NaOH) solution in distilled water was incorporated in Zinc precursor homogenous solution to maintain pH upto 11. Reaction process was allowed for completion at room temperature (27 °C) for 45 min. After obtaining the final form of product, solution was left overnight for settling down the precipitates. The precipitates were separated by

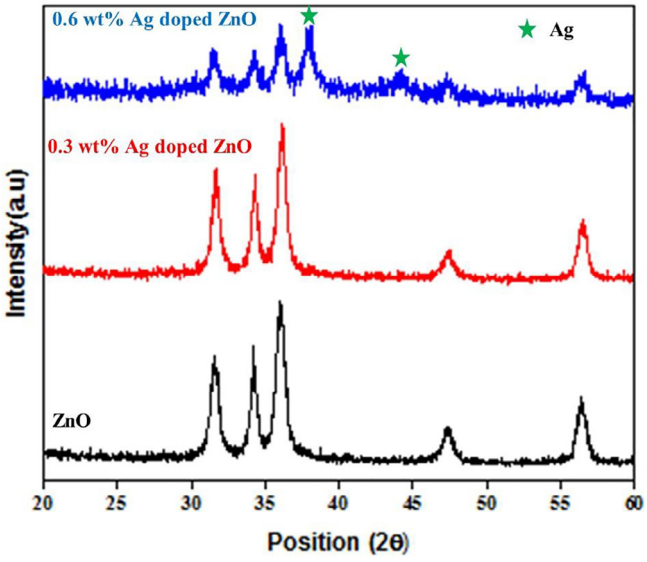


**Fig. 1.** XRD patterns of synthesized nanomaterials; 0.6 wt% silver doping in ZnO NPs presents silver peaks in the diffraction pattern.

**Table 1**
Different calculated structural parameters such as phase identification, relative peak intensity, d-spacing, crystallite size, strain (ε) and dislocation density (δ) of ZnO and Ag doped ZnO nanocrystals.

| Synthesis parameter | Phases | 2($\theta$)Obs | Plane | d-spacing (nm) | Relative Intensity | C.S (nm) | Strain | Dislocation density (*$10^{15}$ lines/$m^2$) |
|---|---|---|---|---|---|---|---|---|
| X = 0 | $Ag_x$-$ZnO_{1-X}$ | 31.54 | (100) | 2.837 | 64.81 | 24.27 | 0.0757 | 1.69 |
| | | 34.16 | (002) | 2.625 | 56.55 | 32.14 | 0.0564 | 0.97 |
| | | 36.14 | (101) | 2.486 | 100 | 11.98 | 0.1496 | 6.96 |
| | | 47.29 | (102) | 1.922 | 21.25 | 13.20 | 0.1261 | 5.74 |
| | | 56.41 | (110) | 1.629 | 37.08 | 7.29 | 0.2115 | 18.82 |
| X = 0.3 | $Ag_x$-$ZnO_{1-X}$ | 31.65 | (100) | 2.827 | 66.35 | 27.73 | 0.0662 | 1.30 |
| | | 34.33 | (002) | 2.613 | 63.75 | 32.12 | 0.0564 | 0.97 |
| | | 36.12 | (101) | 2.487 | 100 | 23.97 | 0.0748 | 1.74 |
| | | 47.38 | (102) | 1.919 | 16.11 | 15.39 | 0.1081 | 4.22 |
| | | 56.43 | (110) | 1.629 | 38.94 | 9.11 | 0.1691 | 12.04 |
| X = 0.6 | $Ag_x$-$ZnO_{1-X}$ | 31.58 | (100) | 2.833 | 55.18 | 16.18 | 0.1136 | 3.82 |
| | | 34.38 | (002) | 2.616 | 53.17 | 19.27 | 0.0940 | 2.69 |
| | | 36.02 | (101) | 2.493 | 100 | 13.70 | 0.1310 | 5.32 |
| | | 37.90 | (111) | 2.374 | 93.81 | 15.90 | 0.1116 | 3.95 |
| | | 44.12 | (200) | 2.053 | 24.1 | 7.79 | 0.2188 | 16.47 |
| | | 47.23 | (102) | 1.925 | 17.89 | 7.70 | 0.2163 | 16.85 |
| | | 56.33 | (110) | 1.632 | 32.55 | 9.11 | 0.1692 | 12.03 |

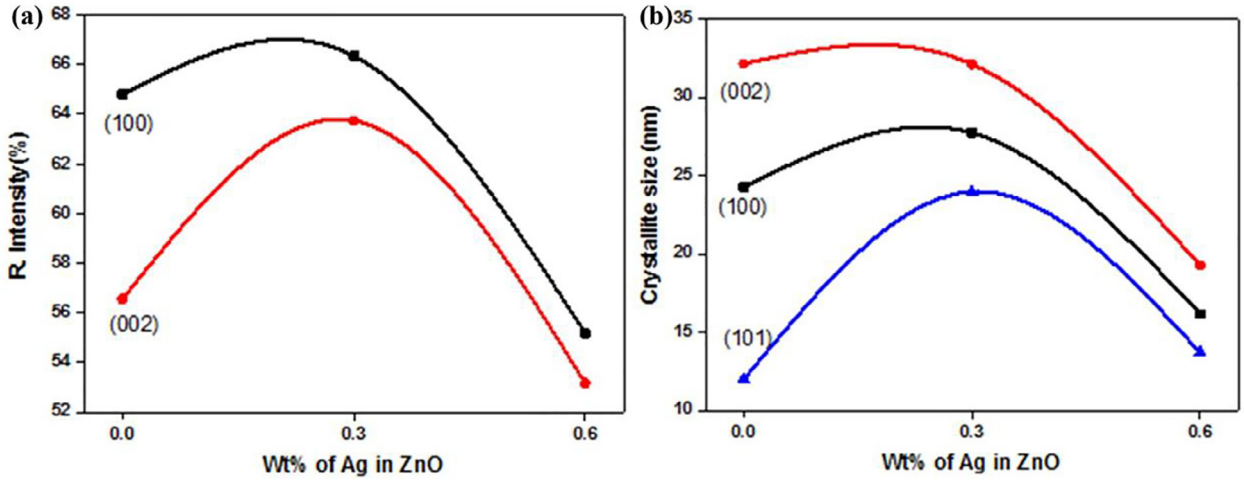


**Fig. 2.** Variation in (a) relative intensity of (100) and (002) planes of synthesized nanomaterials, (b) average crystallite size for different crystalline planes of zinc oxide and silver doped zinc oxide nanomaterials.

centrifugation, washed with water several times and dried in oven at 60 °C for 8 h. Grinding process were performed to obtain the homogenous form of fine particles. For Ag doped ZnO, similar procedure was adopted accept silver source i.e. $AgNO_3$ and zinc acetate were mixed initially in the method.

### 2.2. Characterization

#### 2.2.1. Tools

XRD is performed using a Philips (model Xpert) diffractometer with a Cu Kα X-rays (λ = 0.15406 nm) and 2θ range of 20–60°. Mira3 TESCAN is used for morphology analysis. The FTIR analysis were performed using a Perklin Elmer apparatus of version 10.4.3. PL spectra are recorded at room temperature with excitation at a wavelength of 325 nm.

#### 2.2.2. Structural analysis

Formulae of different calculated structural parameter can be found below (Lam et al., 2018; Kumar et al., 2017).

$$C.S = \frac{\kappa\lambda}{\beta Cos\theta} \tag{1}$$

where k, λ and β are the shape constant (0.9), wavelength of incident Cu $K_\alpha$ radiations (λ = 1.54 Å) and full width at half maximum of corresponding diffraction peak respectively.

The strain (ε) developed is calculated by the relation

$$\varepsilon = \frac{\beta Cos\theta}{4} \tag{2}$$

The dislocation density (δ) is determined by employing the relation

$$\delta = \frac{1}{(C.S)^2} \tag{3}$$

The unit cell dimensions (a, c) are determined by using the relation

$$\frac{1}{d^2_{(hkl)}} = \frac{4}{3}\left(\frac{h^2 + hk + k^2}{a^2}\right) + \frac{l^2}{c^2} \tag{4}$$

And the bond length in ZnO and Ag-ZnO is found by using the relation

$$L = \sqrt{\left(\frac{a^2}{c} + \left(\frac{1}{2} - u\right)^2 c^2\right)} \tag{5}$$

&

$$u = \frac{a^2}{3c^2} + 0.25 \tag{6}$$

### 2.3. Anti-cancer activity

#### 2.3.1. Cytotoxicity on lungs A-549 cancer cells

The dose concentration value of ZnO and Ag-ZnO was calculated using the MTT [3-(4,5 dimethylthiazol-2yl)-2,5-diphenyl tetrazolium bromide] assay. Cell lines were grown in DMEM enhanced with 3 mM L1 glutamine, 100 μ/mL penicillin, 100 mg/ml streptomycin and 15% FBS. The cell culturing process was completed by using 50 $cm^2$ cell culture flasks at 37 °C in incubator. After the culturing process these were shifted in 70 well plates and incubated for 48 h. A-549 lungs cancer cells were treated with various concentration of ZnO and Ag-ZnO NPs (25, 50, 75, 100, 125, 150, 175 and 200 μg/ml). MTT at 5 mg/mL was incorporated in individual well and incubated for 4 h (AlSalhi et al., 2020; Fakhar-e-Alam et al. (2020a), Fakhar-e-Alam et al. (2020b)). When they were dissolved in 100 mL dimethyl sulfoxide (DMSO), purple color crystals were

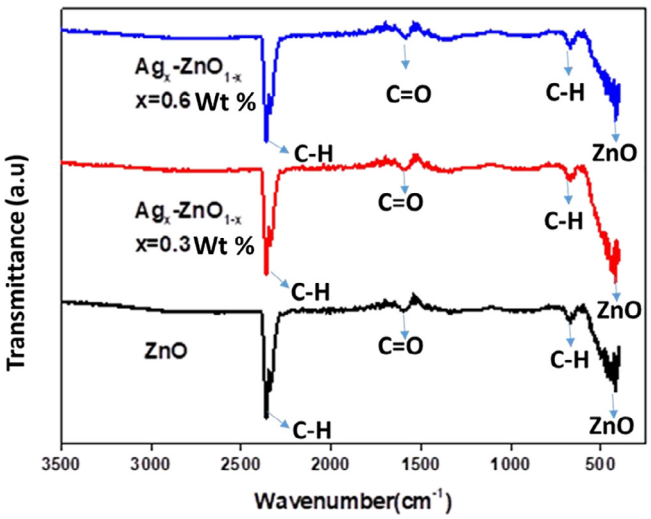


**Fig. 3.** FTIR spectra of ZnO and Ag doped ZnO nanomaterials.

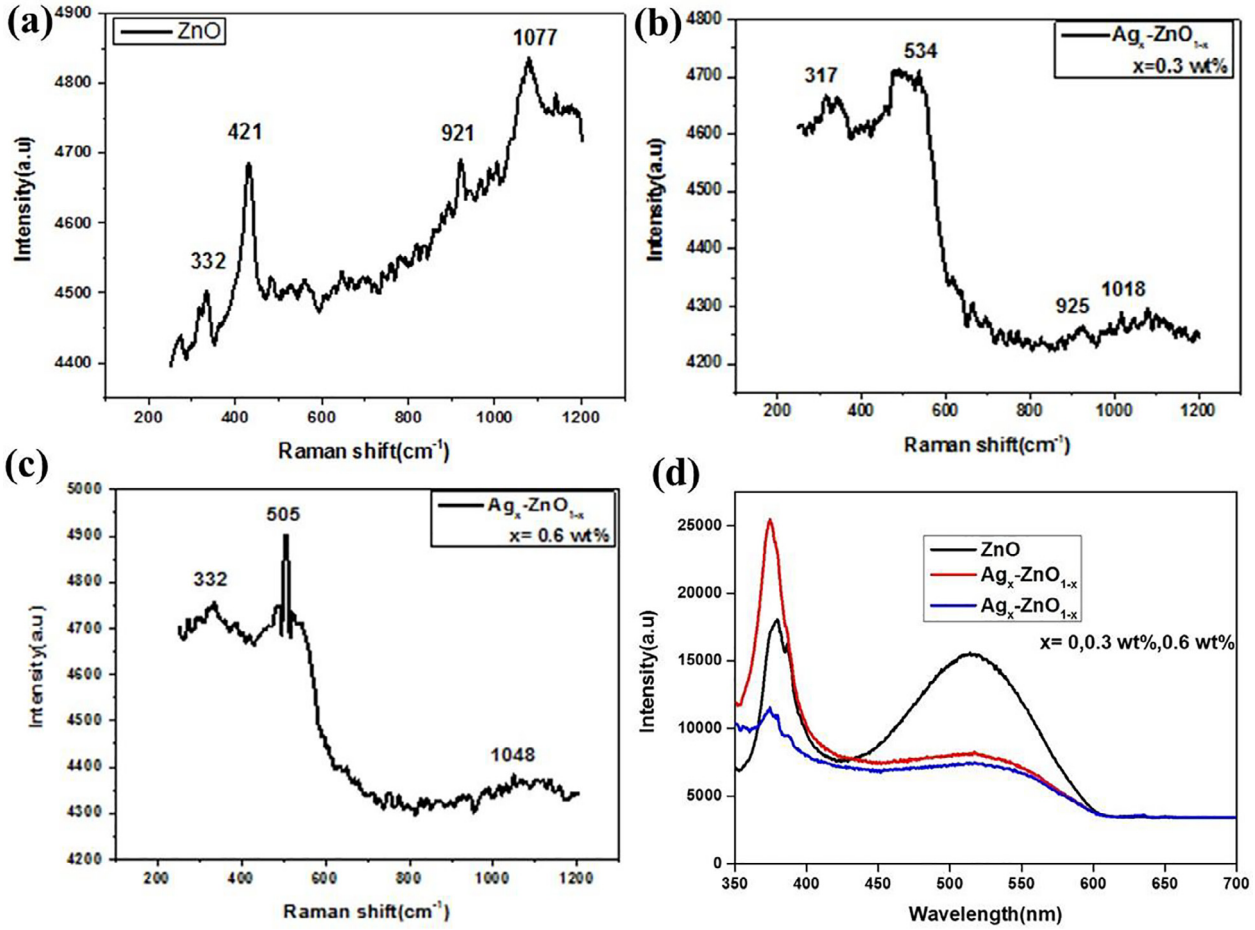


**Fig. 4.** Raman Spectra of (a) ZnO, (b) 0.3 wt% and (c) 0.6 wt% Ag doped ZnO nanomaterials, (d) Photoluminescence spectra of synthesized nanomaterials presenting different optical absorption peaks.

formed. The optical density calculated at 570 nm and then cell viability was calculated by formula:

$$\text{Cell viability}\% = (\text{OD values of experimental sample}/\text{OD values of experimental control}) * 100$$

## 3. Results and discussion

Fig. 1 shows the XRD patterns of ZnO and Ag doped ZnO NPs synthesized by co-precipitation method (0.3 and 0.6 wt%). The diffraction peaks appeared at 2θ values of 31.54°, 34.16°, 36.14°, 47.29° and 56.41° are related to hexagonal wurtzite ZnO structure. It is found that no diffraction peak is observed related to Ag up to x = 0.3 wt%, while the diffraction peaks of Ag are appeared at 2θ values of 37.9° and 44.12° belong to (111) and (200) planes for x = 0.6 wt%.

Fig. 2a exhibits relative peak intensity relation of (100) and (002) planes of ZnO and Ag doped ZnO NPs. The relative peak intensity of (100) and (002) planes is increased up to 0.3 wt% of Ag content whereas it is decreased with the further increase of Ag (0.6 wt%) atoms. The increase in relative peak intensity of said planes indicates the growth of ZnO NPs which is due to the incorporation of lower amount of Ag (0.3 wt%). When the amount of Ag is increased to 0.6 wt%, the FWHM of (100), (002) planes is increased causes to develop micro-strains, point defects and stresses. In short, the relative peak intensity is associated with the rise of silver contents (Kirchlechner et al., 2010). The growth of Ag doped ZnO NPs is more along (100) orientations because the peak intensity of these planes is greater than other ZnO peaks (Karyaoui et al., 2015).

Fig. 2b reveals the variation in crystallite size of (100), (002) and (101) crystalline planes of pristine and Ag doped ZnO NPs prepared by co-precipitation method. The crystal size for (101) plane is increased significantly while it is slightly increased for (100) and (002) planes at 0.3 wt% of Ag in ZnO NPs. Interestingly, the crystallite size of all the planes are decreased at 0.6 wt%. Results show that the lower (0.3 wt%) content of Ag increases the crystal growth while the higher content (0.6 wt%) of Ag discourages the crystal formation. This decrease in crystal growth is evident with the increase of FWHM and the development of micro-strains and point defects. Moreover, the increase in crystal growth indicates the stress relaxation while the decrease in crystal growth indicates the emergence of irregularities in the crystal due to crystalline defects. These crystalline defects can cause the shrinking or elongation of lattice parameters, d-spacing and hence distorted the crystal lattice.

Due to shifting in diffraction peaks, the d-spacing values are varied with the change in concentration. The d-spacing of (100) and (002) planes is decreased for 0.3 wt% of Ag while it is increased for 0.6 wt%. There is a direct relationship between crystallite size, strain and d-spacing for (100) and (002) planes with the increase of Ag contents. On the other hand, there is no variation in these structural parameters for (101) plane which indicate that the silver addition does not affect the growth orientation of ZnO NPs.

The cell parameters a and c are increased with increasing of Ag (0.6 wt%) concentration in ZnO NPs. The estimated values of lattice

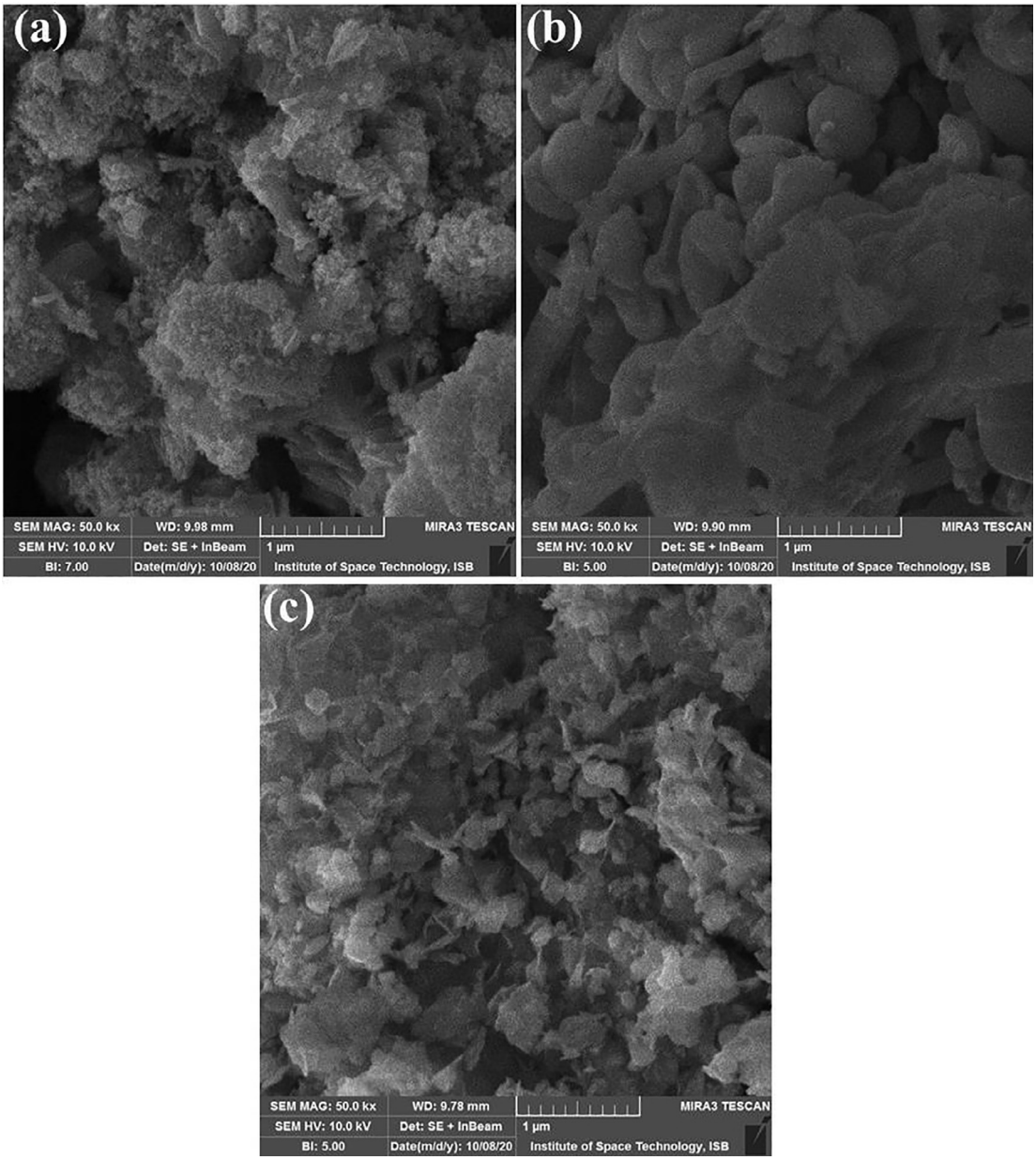


**Fig. 5.** SEM images of synthesized nanomaterials (a) ZnO (b) 0.3%wt Ag doped ZnO (c) 0.6%wt Ag doped ZnO nanostructures.

parameter are very close to their standard values ($a$ = 0.325 and $c$ = 0.521 nm), however the small variation in lattice parameters is due to Ag doping in ZnO NPs. The "$L$" bond length also increased with increasing the Ag concentration.

FTIR spectra of ZnO NPs with contents of Ag (0.3%, 0.6%wt) are shown in Fig. 3. Synthesized NPs possess different organic species attached to the NPs at different wavenumbers. The IR spectra are recorded in the range 400–3500 $cm^{-1}$. The peak appeared at 2362 $cm^{-1}$ is determined as the symmetric and asymmetric broadening vibrations of C–H functional groups. The band present at 1588 $cm^{-1}$ indicates C═O stretching bond. The medium to weak band at 670 $cm^{-1}$ is attributed to the change in nanostructured characteristics upon silver addition into Zn–O lattice. The spectrum obtained clearly displays ZnO band at 418 $cm^{-1}$ in the form of metal oxygen bonding.

The ZnO has wurtzite hexagonal structure with eight types of optical modes situated at the middle of Brillouin zone (Γ point).

$$\Gamma = 1A1 + 2B1 + 1E1 + 2E2$$

where A1 and E1 Brillouin zones belong to two polar branches. These Brillouin zones are split into longitudinal and transversal optical parts containing varied frequencies owing to macroscopic electric fields of LO phonons. In case of nonpolar E2, modes as a low frequency mode (E2L) are assigned with the Zn sub-lattice. In other case only oxygen atoms involve with high frequency mode (E2H). Due to inactiveness of B1 mode, this is known as silent mode. The Raman spectra of the nanomaterials were determined from 200 $cm^{-1}$ to 1200 $cm^{-1}$ at room temperature (Fig. 4a–c). Raman spectrum of ZnO NPs contains four peaks aroused at 332, 421, 921 and 1077 $cm^{-1}$. These observed peaks belong to the E2L, A1, E2H and A1 (LO) Brillouin zone of hexagonal ZnO (Zeferino et al., 2011) respectively. The spectra of Ag doped ZnO leads to the lower mode of A1 (LO) and observe peaks shifted about 15 $cm^{-1}$ towards lower angles. Furthermore, in A1 (LO) phonon mode observed peaks shift and broadening due to scattering. The peaks are appeared at

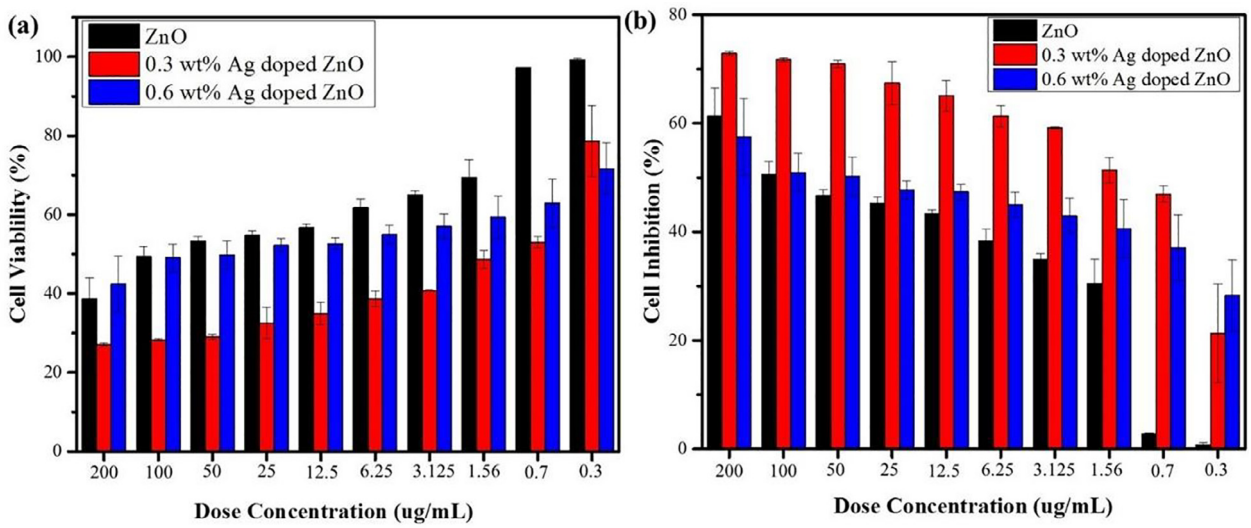


**Fig. 6.** Cell viability and inhibition of A549 cells with different doses of ZnO and Ag-doped ZnO nanomaterials.

317, 534, 925 and 1018 $cm^{-1}$ outside the center of Brillouin zone. The lower phonon mode A1 (LO) is conventionally evaluated the oxygen vacancies, the defect complexes usually contain O vacancy in Zn interstitial. however, the Ag concentration increase the shifting towards the higher frequencies and the peaks appeared at the 332, 505 and 1048 $cm^{-1}$ (Sathya et al., 2017). Moreover, with increasing the Ag concentration, the broad Raman peak is appeared at 505 $cm^{-1}$ due to surface interface phonon mode. The Ag effect on ZnO spectra can be witnessed with peak at 317 $cm^{-1}$. PL spectroscopy have been probed optical properties of the nanomaterials. The PL peak is appeared at around 380 nm in the case of ZnO. Due to doping of Ag (0.3% and 0.6% wt) peak shifted to the lower angle at 373 nm (Fig. 4d). The emission band is attributed to unbound exciton recombination in ZnO NPs. The emission peak of pristine and Ag doped ZnO are observed at about 458–583 nm in the visible range (Sathya et al., 2017). Due to intrinsic and extrinsic imperfections, ZnO can emit visible emission. The creation of defects is related to the incorporation of silver in ZnO NPs (Zeferino et al., 2011).

The morphology of the NPs is dependent on the synthesis methods and crystal formation. The surface morphology of the crystal is observed by SEM. SEM images show the grain nanocrystalline morphology and well controlled structure (Fig. 5a). There are many smaller particles are visible indicating the formation of nanosized particles. In case of 0.3 wt% of silver doping, larger aggregates can be observed (Fig. 5b), whereas 0.6 wt% doping presents flake like morphologies (Fig. 5c).

The biomedical importance of silver and zinc oxide NPs in evident in the literature for cancer treatments (Baghbani-Arani and Shandiz, 2020; Cheng et al., 2020; Huy et al., 2020). By using MTT assay, anticancer behavior is determined for the A549 (lung

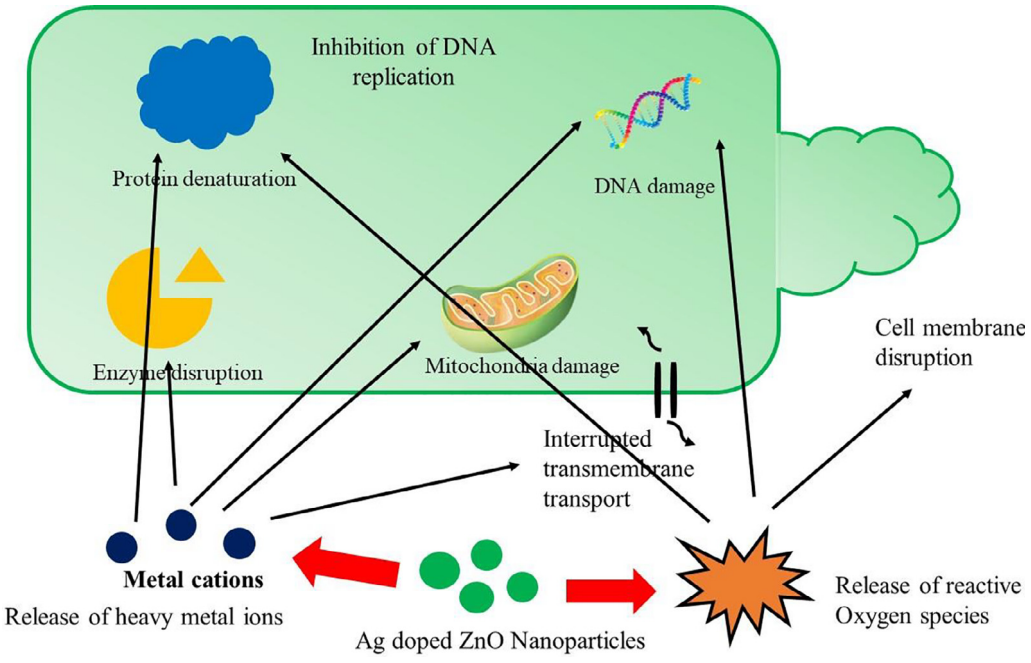


**Fig. 7.** Proposed mechanisms i.e. ROS generation and metal ions release showing cell inhibition due to silver doped ZnO nanomaterials.

cancer cell line). The anti-cancer activities with dose concentrations from 0.3 to 200 μg/mL are evaluated after 48 h incubation time. The cytotoxic activity of these NPs are dose dependent against A549 cell lines.

The outcome performance of $Ag_xZnO_{1-x}$ (x = 0.3 wt%) NPs induced more cell lethality in A549 cells as compared to ZnO, $Ag_x$-$ZnO_{1-x}$ (x = 0.6 wt%) NPs (Fig. 6a).

ZnO and $Ag_x$-$ZnO_{1-x}$ NPs induce dose dependent inhibition for different materials as shown in Fig. 6b. It is observed that cell inhibition decreases at lower dose concentration. When compare the cell death rate between 0.3 wt% and 0.6 wt%, cell inhibition remain on higher side for 0.3 wt% at different doses and its ratio remain almost one fourth time higher from dose concentration 0.7 to 100 μg/mL. The $Ag_x$-$ZnO_{1-x}$ (x = 0.3 wt%) NPs exhibited the highest cell inhibition 72.86 % at concentration 200 μg/mL. The important phenomena behind the anti-cancer effect of $Ag_x$-$ZnO_{1-x}$ (x = 0.3) NPs are production of ROS because of releasing ions (Pandiyan et al., 2019). The higher anticancer effect of $Ag_x$-$ZnO_{1-x}$ (x = 0.3), NPs is related to the releasing of silver and zinc ions to breed the ROS. The ROS penetrate through cell membrane and cause cell damage.

The cytotoxicity mechanism of $Ag_x$-$ZnO_{1-x}$ (x = 0.3 wt%) NPs can be due to ROS generation, oxidative stress, and introduction of apoptosis which cause damage of majority of A549 lungs cancer cells. The physical properties of $Ag_x$-$ZnO_{1-x}$ (x = 0.3 wt%) NPs also play a vital role in cytotoxic effect such as crystallite size, dose rate, size distribution, surface functionalization of materials, and processing kinetics. Higher cytotoxic effects were shown by the small size of the NPs. These NPs are effortlessly penetrated the lungs cells to generate the ROS which cause cell death. The results of $Ag_x$-$ZnO_{1-x}$ (x = 0.3 wt%) were showed that dose dependent study had reduced the cell viability of A549 cell lines. The $Ag_x$-$ZnO_{1-x}$ (x = 0.3 wt%) NPs penetrate the cells and damages the cancer cell function. The important phenomena is that, the small energy band gap materials absorb the energy from sun light and destroy the cell membrane of cancer cells. Another important parameter for the A549 cancer cell death is the charge on the metal ions. It was determined that for increasing the efficiency against the cancer cells, NPs generate the positive charge i.e., $Ag^+$, $Zn^{2+}$ and due to ionic interactions, cell membrane were negatively charged (Fig. 7). Due to the charge effect, the attraction produce between the positive and negative charge and the position of attraction towards the negatively charged cell membrane. The $Ag_xZnO_{1-x}$ (x = 0.3 wt%) NPs interact actively with negatively charged surface of cancer cell membrane, cause cell membrane breakage and destroy cancerous cells. This phenomenon follows liberation of silver and zinc ions intracellularly which is more effective against cytotoxicity and enzyme disruption. This shows that $Ag_xZnO_{1-x}$ (x = 0.3 wt%) NPs can be a potential candidate with improved efficacy against cancerous cells (Pandiyan et al., 2019).

## 4. Conclusion

In this research work, effect of silver doping on zinc oxide structure has been evaluated. Silver with 0.3 wt% and 0.6 wt% are doped in zinc oxide and structural, optical, bonding and morphological properties are studied. Two addition peaks of silver are observed in 0.6 wt% doped ZnO. Morphology of the nanomaterials is also affected by doping and NPs transform into flake like shapes. PL absorption spectra of synthesized nanomaterials have shown blue shift upon doping of silver atoms. Anticancer potential of nanomaterials has shown that 0.3 wt% have higher cell inhibition rate as compare to pristine or 0.6 wt% silver doped Zinc oxide. This study has shown that silver doping can significantly enhance the anticancer activity of zinc oxide nanomaterials.

## Funding

This work was financially supported by Higher Education Commission Pakistan under NRPU project No. 6411.

## Declaration of Competing Interest

The authors declare that they have no known competing financial interests or personal relationships that could have appeared to influence the work reported in this paper.

## References

AlSalhi, M.S., Aziz, M.H., Atif, M., Fatima, M., Shaheen, F., Devanesan, S., Aslam Farooq, W., 2020. Synthesis of NiO nanoparticles and their evaluation for photodynamic therapy against HeLa cancer cells. J. King Saud Univ.-Sci. 32 (2), 1395–1402.

Baghbani-Arani, F., Shandiz, S.A.S., 2020. Combination of Cytochalasin H and zinc oxide nanoparticles in human breast cancer: an insight into apoptosis study. Biologia, 1–10.

Beyene, H.D., Werkneh, A.A., Bezabh, H.K., Ambaye, T.G., 2017. Synthesis paradigm and applications of silver nanoparticles (AgNPs), a review. Sust. Mater. Tech. 13, 18–23.

Caglar, M., Yakuphanoglu, F., 2012. Structural and optical properties of copper doped ZnO films derived by sol–gel. Appl. Surf. Sci 258 (7), 3039–3044.

Castro-Lopes, S., Guerra, Y., Silva-Sousa, A., Oliveira, D., Gonçalves, L., Franco, A., Padrón-Hernández, E., Peña-Garcia, R., 2020. Influence of pH on the structural and magnetic properties of Fe-doped ZnO nanoparticles synthesized by sol gel method. Solid State Sci. 109, 106438.

Chauhan, R., Kumar, A., Chaudhary, R.P., Education, T., 2010. Synthesis and characterization of silver doped ZnO nanoparticles. Arch. Appl. Sci. Res 2 (5), 378–385.

Chen, Y., Liu, Y., Lu, S., Xu, C., Shao, C., Wang, C., Zhang, J., Lu, Y., Shen, D., Fan, X., 2005. Optical properties of ZnO and ZnO: In nanorods assembled by sol-gel method. J. Chem. Phys. 123, (13) 134701.

Chen, Y., Tse, W.H., Chen, L., Zhang, J., 2015. Ag nanoparticles-decorated ZnO nanorod array on a mechanical flexible substrate with enhanced optical and antimicrobial properties. Nanoscale Res. Lett. 10 (1), 1–8.

Cheng, J., Wang, X., Qiu, L., Li, Y., Marraiki, N., Elgorban, A.M., Xue, L., 2020. Green synthesized zinc oxide nanoparticles regulates the apoptotic expression in bone cancer cells MG-63 cells. J. Photochem. Photobiol. B, Biol. 202, 111644.

Fakhar-e-Alam, M., Aseer, M., Rana, M.S., Hammad Aziz, M., Atif, M., Yaqub, N., Farooq, W.A., 2020a. Spectroscopic features of PHOTOGEM® in human Rhabdomyosarcoma (RD) cellular model. J. King Saud Univ.-Sci. 32 (7), 3131–3137.

Fakhar-e-Alam, M., Aqrab-ul-Ahmad, Atif, M., Alimgeer, K.S., Suleman Rana, M., Yaqub, N., Aslam Farooq, W., Ahmad, H., 2020b. Synergistic effect of TEMPO-coated TiO2 nanorods for PDT applications in MCF-7 cell line model. Saudi J. Biol. Sci. 27 (12), 3199–3207.

Golego, N., Studenikin, S., Cocivera, M., 2000. Sensor photoresponse of thin-film oxides of zinc and titanium to oxygen gas. J. Electrochem. Soc 147 (4), 1592.

Herng, T., Lau, S., Yu, S., Yang, H., Wang, L., Tanemura, M., Chen, J., 2007. Magnetic anisotropy in the ferromagnetic Cu-doped ZnO nanoneedles. Appl. Phys. Lett. 90, (3) 032509.

Huy, T.Q., Huyen, P., Le, A.-T., Tonezzer, M., 2020. Recent advances of silver nanoparticles in cancer diagnosis and treatment. Anti-Cancer Agents Med. Chem. (Formerly Current Medicinal Chemistry-Anti-Cancer Agents) 20 (11), 1276–1287.

Karyaoui, M., Mhamdi, A., Kaouach, H., Labidi, A., Boukhachem, A., Boubaker, K., Amlouk, M., Chtourou, R., 2015. Some physical investigations on silver-doped ZnO sprayed thin films. Mater. Sci. Semicond. Process. 30, 255–262.

Kaur, A., Ibhadon, A.O., Kansal, S.K., 2017. Photocatalytic degradation of ketorolac tromethamine (KTC) using Ag-doped ZnO microplates. J. Mater. Sci. 52 (9), 5256–5267.

Keren, K., Berman, R.S., Buchstab, E., Sivan, U., Braun, E., 2003. DNA-templated carbon nanotube field-effect transistor. Science 302 (5649), 1380–1382.

Kirchlechner, C., Martinschitz, K., Daniel, R., Klaus, M., Genzel, C., Mitterer, C., Keckes, J., 2010. Residual stresses and thermal fatigue in CrN hard coatings characterized by high-temperature synchrotron X-ray diffraction. Thin Solid Films 518 (8), 2090–2096.

Kumar, V., Prakash, J., Singh, J.P., Chae, K.H., Swart, C., Ntwaeaborwa, O., Swart, H., Dutta, V., 2017. Role of silver doping on the defects related photoluminescence and antibacterial behaviour of zinc oxide nanoparticles. Colloids Surf. B: Biointerfaces 159, 191–199.

Lam, S.-M., Quek, J.-A., Sin, J.-C., 2018. Mechanistic investigation of visible light responsive Ag/ZnO micro/nanoflowers for enhanced photocatalytic performance and antibacterial activity. J. Photochem. Photobiol. A 353, 171–184.

Mohan, R., Ravichandran, K., Nithya, A., Jothivenkatachalam, K., Ravidhas, C., Sakthivel, B., 2014. Influence of spray flux density on the photocatalytic activity and certain physical properties of ZnO thin films. J. Mater. Sci. Mater. Electron. 25 (6), 2546–2553.

Nagaraju, G., Prashanth, S., Shastri, M., Yathish, K., Anupama, C., Rangappa, D., 2017. Electrochemical heavy metal detection, photocatalytic, photoluminescence, biodiesel production and antibacterial activities of Ag–ZnO nanomaterial. Mater. Res. Bull. 94, 54–63.

Nakada, T., Hirabayashi, Y., Tokado, T., Ohmori, D., Mise, T., 2004. Novel device structure for Cu (In, Ga) Se2 thin film solar cells using transparent conducting oxide back and front contacts. Sol. Energy 77 (6), 739–747.

Naskar, A., Jana, B., Kim, H.G., Kwac, L.K., 2019. Hydrazine mediated low temperature soft chemical synthesis of mixed metal oxide (γ-Fe2O3–ZnO) graphene nanocomposite: in vitro cytotoxicity study on HeLa and SK-BR-3 cell lines. Mater. Res. Express 6, (8) 085019.

Neto, N.A., Matsui, K., Paskocimas, C., Bomio, M., Motta, F., 2019. Study of the photocatalysis and increase of antimicrobial properties of Fe3+ and Pb2+ co-doped ZnO nanoparticles obtained by microwave-assisted hydrothermal method. Mater. Sci. Semicond. Process 93, 123–133.

Nomura, K., Ohta, H., Ueda, K., Kamiya, T., Hirano, M., Hosono, H., 2003. Thin-film transistor fabricated in single-crystalline transparent oxide semiconductor. Science 300 (5623), 1269–1272.

Pal, K., Maiti, U.N., Majumder, T.P., Debnath, S.C., Bennis, N., Otón, J.M., 2013a. Synthetic strategy of porous ZnO and CdS nanostructures doped ferroelectric liquid crystal and its optical behavior. J. Mol. Struct. 1035, 76–82.

Pal, K., Pal Majumder, T., Schirhagl, R., Ghosh, S., Roy, S.K., Dabrowski, R., 2013b. Efficient one-step novel synthesis of ZnO nanospikes to nanoflakes doped OAFLCs (W-182) host: Optical and dielectric response. Appl. Surf. Sci. 280, 405–417.

Pal, K., Mohan, M.M., Zhan, B., Wang, G., 2015. Design, synthesis and application of hydrogen bonded smectic liquid crystal matrix encapsulated ZnO nanospikes. J. Mater. Chem. 3 (45), 11907–11917.

Pandiyan, N., Murugesan, B., Arumugam, M., Sonamuthu, J., Samayanan, S., Mahalingam, S., 2019a. Ionic liquid-A greener templating agent with Justicia adhatoda plant extract assisted green synthesis of morphologically improved Ag-Au/ZnO nanostructure and it's antibacterial and anticancer activities. J. Photochem. Photobiol. B, Biol. 198, 111559. https://doi.org/10.1016/j.jphotobiol.2019.111559.

Pandiyan, N., Murugesan, B., Sonamuthu, J., Samayanan, S., Mahalingam, S., 2019b. [BMIM] PF6 ionic liquid mediated green synthesis of ceramic SrO/CeO2 nanostructure using Pedalium murex leaf extract and their antioxidant and antibacterial activities. Ceram. Int. 45 (9), 12138–12148.

Pearton, S., Heo, W., Ivill, M., Norton, D., Steiner, T., 2004. Dilute magnetic semiconducting oxides. Semicond. Sci. Technol. 19 (10), R59.

Ravichandran, K., Sathish, P., Snega, S., Karthika, K., Rajkumar, P., Subha, K., Sakthivel, B., 2015. Improving the antibacterial efficiency of ZnO nanopowders through simultaneous anionic (F) and cationic (Ag) doping. Powder Technol. 274, 250–257.

Sagadevan, S., Pal, K., Chowdhury, Z.Z., Hoque, M.E., 2017. Structural, dielectric and optical investigation of chemically synthesized Ag-doped ZnO nanoparticles composites. J. Sol-Gel Sci. Technol. 83 (2), 394–404.

Sathya, B., Anburaj, D.B., Porkalai, V., Nedunchezhian, G., 2017. Raman scattering and photoluminescence properties of Ag doped ZnO nano particles synthesized by sol–gel method. J. Mater. Sci. Mater. Electron. 28 (8), 6022–6032.

Sundaram, P.S., Inbanathan, S.S.R., Arivazhagan, G., 2019. Structural and optical properties of Mn doped ZnO nanoparticles prepared by co-precipitation method. Phys. B Condens. Matter 574, 411668.

Wang, X., Song, J., Liu, J., Wang, Z.L., 2007. Direct-current nanogenerator driven by ultrasonic waves. Science 316 (5821), 102–105.

Wang, Z., Kong, X. 2004. Y, Ding, P. Gao, WL Hughes, R. Yang, Y. Zhang. Adv. Funct. Mater. 14, 943.

Zeferino, R.S., Flores, M.B., Pal, U., 2011. Photoluminescence and Raman scattering in Ag-doped ZnO nanoparticles. Int. J. Appl. Phys. 109, (1) 014308.